Fixed-axis electric sail deployment dynamics analysis using hub-mounted momentum control

JoAnna Fulton [*], Hanspeter Schaub

University of Colorado at Boulder, 431 UCB, Colorado Center for Astrodynamics Research, Boulder, CO 80309-0431, USA

A B S T R A C T

The deployment dynamics of a spin stabilized electric sail (E-sail) with a hub-mounted control actuator are investigated. Both radial and tangential deployment mechanisms are considered to take the electric sail from a post-launch stowed configuration to a fully deployed configuration. The tangential configuration assumes the multi-kilometer tethers are wound up on the exterior of the spacecraft hub, similar to yo-yo despinner configurations. The deployment speed is controlled through the hub rate. The radial deployment configuration assumes each tether is on its own spool. Here both the hub and spool rate are control variables. The sensitivity of the deployment behavior to E-sail length, maximum rate and tension parameters is investigated. A constant hub rate deployment is compared to a time varying hub rate that maintains a constant tether tension condition. The deployment time can be reduced by a factor of 2 or more by using a tension controlled deployment configuration.

1. Introduction

The E-sail is a novel propellantless in-space propulsion concept with great potential for fast interplanetary and near interstellar missions, invented and proposed by Pekka Janhunen [1] at the Finnish Meteorological Institute. In this concept, a system of radially configured, thin, charged tethers generate an electric field that interacts with solar wind protons to harvest acceleration for spacecraft propulsion, demonstrated in Fig. 1. This provides infinite specific impulse and eliminates the need for traditional chemical propellants [2]. Only an electron gun is required to maintain a positive electrostatic charge on the tethers. The positive solar wind ions deflect of the results E-sail tether force field, causing a net force onto the spacecraft. This solar wind propulsion concept is advantageous in comparison to the solar radiation pressure (SRP) based solar sail due to the effective area of the electrostatic forces and improved solar radius dependence [3]. A single charged wire, microns thick, will create a meters-wide effective area, expanding the area of influence of a minimal structure. In comparison, SRP is directly dependent on the physical area of the solar sail, providing many challenges in manufacturing, packaging, and deploying large membranes [4]. The solar radius dependence of the E-sail has been shown to decay the acceleration at $1/r^{7/6}$, slower than that of the solar sail at $1/r^2$. This is encouraging for long distance missions to the outer planets and beyond. However, the E-sail is not operable within a planet's magnetosphere, where the solar wind protons are

deflected, whereas a solar sail still accelerates on the photons in this region.

Multiple missions have been designed using the E-sail as the primary propulsion system with encouraging results. A fast entry probe mission to Uranus could be achieved in less than 6 years [5], the interstellar medium reached in as little as 10 years, and a near Earth asteroid rendezvous could be completed within a year [6]. Additionally, missions to the inner planets, such as Venus and Mars, could also be achieved in less than 1 and 2 years, respectively [7]. This provides adequate motivation to pursue further development of the E-sail system. The electrostatic propulsion theory enabling these missions has been studied in detail [3,8]. Additionally, work has been done concerning the sail shape under thrust [9] and for solving secular drift in the operating sail spin rate using only voltage modulation [10]. However, the coupled deployment dynamics of the spacecraft and charged tether system is not well understood. Typically, the E-sail systems considered are composed of 20–100 tethers, up to 20 km in length, with payload masses of 100–2000 kg. These tethers are constructed using multiple micron-thick conductive tethers with auxiliary loops, known as a Hoytether [11], to provide redundancy and protect against micrometers. Construction of such tethers at the desired length has been investigated with encouraging results [12]. One such tether, 10 m in length, was flown on the EstCube-1 [13] but was not deployed [14]. Despite this, evidence supporting the feasibility of the E-sail is continuing to develop, and steps should now be taken towards

* Corresponding author.
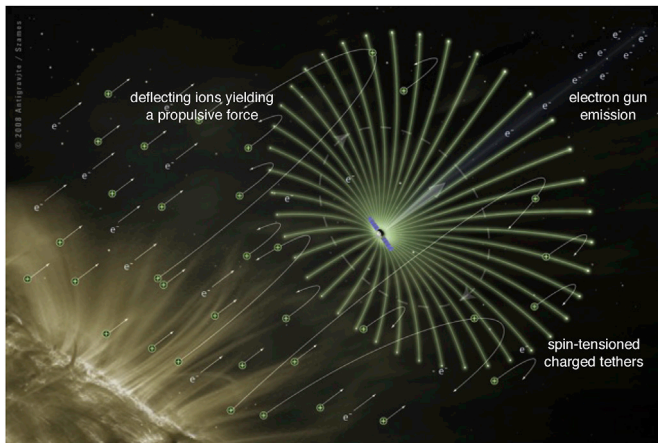 *E-mail address:* joanna.fulton@colorado.edu (J. Fulton).

Fig. 1. The electric sail is charged by a spin axis-pointed electron beam and deflects solar wind protons to generate thrust. Artist concept image by A. Szames.

understanding the deployment requirements for such a structure.

During flight, the tethers are spin-stabilized to maintain tensioned, radial, straight line configurations. Therefore, at the end of the deployment phase, the spacecraft and each tether component must be rotating at equal rates. This can be achieved through either a centrifugal deployment or by actuating the tethers from rest using tether-mounted thrust and spinning up the tethers and spacecraft after the tethers are fully extended. In this paper, only a centrifugal deployment is considered. Due to conservation of momentum, a centrifugally deployed tether system modeled with a spherical pendulum (such as a yo-yo despinner) asymptotically approaches the negative initial rate when left in free spin. This fact can be leveraged for deployment by adjusting the tether length or initial rate such that the final desired rate is reached, however for cases where the tether length and system inertia is exceedingly large and predetermined, such as the E-sail, the initial rate required is not practical. For those cases, energy and momentum must be continually input to the system as the tethers are deploying to maintain desired body rates. The primary challenge for a centrifugal E-sail deployment is providing the momentum required to spin-stabilize the deployed structure while minimizing risk and fuel consumption, presenting a non-trivial task.

Review of the literature reveals that many tethered space system concepts have been presented and studied in the past, however none quite resemble the structure proposed here. Kilometers-long space tethers that have flown as of 2016 were single tether missions, such as in the TSS, SEDS, and TiPS missions [15]. These single tether systems used gravity gradients to actuate deployment and hosted much larger payloads, making them poor analogs for the E-sail deployment dynamics. Spin stabilized, multiple-tether systems have been proposed and studied, such as the Terrestrial Planet Finder (TPF) and Submillimeter Probe of the Evolution of Cosmic Structure (SPECS) concepts, however the deployment requirements of these concepts are not necessarily comparable to the E-sail. The SPECS mission, for example, proposes to leverage conservation of momentum during deployment of the 3 tethers by pre-spinning the system to 90 rpm in order to approach 0.01 rpm at full deployment [16]. A quick calculation shows that a pre-spin method will not be feasible for the E-sail deployment. Where an E-sail accelerating a spacecraft at 1 mm/s^2 could easily have an inertia of 10^8 kg m^2, and the rotation rate is limited by the tension capability of the tether and end mass size, the required pre-spin rate could be on the order of 10^5 rpm. Another space structure that somewhat relates to the E-sail is that of wire booms for science payloads, as flown on THEMIS, RBSP, and MMS. However deployment here is also not directly comparable, where the wire lengths are on the order of tens of meters, and therefore do not present the same momentum challenges as the E-sail. These systems also use a spin-up strategy to take advantage of conservation of momentum during deployment [17,18], and therefore offer little additional insight for E-sail deployment solutions.

In this paper novel deployment schemes are studied where the spacecraft body rate is controlled using body-mounted devices. A body-mounted strategy will be simpler than coordinating and commanding individual tether-mounted devices to actuate deployment. Furthermore, applying torque through the hub may be possible using commercially available products, whereas tether end point thruster units are currently under development. Two deployment schemes that use a body-mounted energy source are considered. The first is a tangentially aligned deployment, where all tethers are mounted on a central hub oriented with the spacecraft spin axis, taking advantage of the rotational dynamics to deploy the tethers simultaneously. The second deployment scheme uses a radially oriented deployment configuration. Such a configuration has each tether housed on a separate spool and motor device. This paper compares the dynamic deployment behavior of these two methods. In previous work by the authors [19], the coupled rotational dynamics of the spacecraft and E-sail system was modeled during the deployment phase and initial control of these dynamics was investigated. This paper continues and expands this work through parameter sensitivity analysis and additional control schemes.

A proposed scheme for the E-sail mounts the tethers at a radial orientation [20], where each tether is housed with an individual hub and motor subsystem to conduct the tether reeling. An auxiliary tether would line the periphery of the sail, and thruster units would interface between the tether end points and auxiliary tether to control position and momentum. These components significantly increase the mass budget of the E-sail and introduce a highly complex dynamics problem. In this paper, an auxiliary tether is not included such that only a stand alone end mass is accounted for. Additionally, the deployment is assumed to occur in a single plane, reducing the problem to rotational degrees of freedoms about the deployment normal axis and ignoring out of plane dynamics. It is also assumed that the spacecraft has reached deep space conditions before initiating deployment, the sail is not charged during deployment, and the tethers do not adhere to each other as they deploy. Of interest is the nominal performance for each deployment type, as well as the sensitivity of this performance with respect to the body rate and spool reel rate. Numerical simulations demonstrate the expected performance.

2. E-sail dynamics modeling

2.1. Spacecraft and E-Sail mass model

The mass budget of the E-sail and spacecraft system is selected such that the characteristic acceleration of the E-sail at 1 Au from the Sun is between $a_\oplus = 0.1 - 1$ mm s^{-2}. At $a_\oplus = 1$ mm s^{-2}, significantly faster missions to the outer planets and beyond are feasible [5]. The characteristic acceleration is given by [20]:

$$a_\oplus = \frac{fNL}{m} \tag{1}$$

where N is the number of tethers, L is the length of the tethers, m is the total mass of the spacecraft, and f is the thrust per unit tether length at 1 AU from the Sun. Using the physical reference data for the E-sail [20], this is known to be $f = 579.84$ nN m^{-1} for an E-sail operating at 25 kV nominal tether voltage. The total system mass is set to $m = 500$ kg, a smaller but feasible mass for an interplanetary science mission, to facilitate greater focus on the other free parameters of the system. It is assumed that the maximum number of tethers is 100 and the maximum length of a tether is restricted to 20 km [20]. However, this only slightly restricts the range of E-sail sizes that will yield the desired characteristic acceleration in Eq. (1). For a scenario where there is minimal end mass, no remote devices, and minimal number of tethers with maximum length, the tethers themselves are the largest contribution to the spacecraft system momentum. Therefore, accurate modeling of the E-sail deployment requires that the tether inertia is not treated as negligible.

Here, the tether is modeled as a length-varying slender rod with mass equal to the current tether mass. The tether mass is described as a function of the deployment length, where the mass per unit length per tether is assumed to be $\lambda = 1.155 \times 10^{-5}$ kg/m [20]. Where ρ is the mass per unit length for N number of tethers, $\rho = N\lambda$ for a given sail size. The mass of all deploying tethers is then described as:

$$m_T = \rho l = \rho R\phi \qquad (2)$$

where l is the length as a function of time, which can be described in terms of the unwrap angle ϕ and the spacecraft hub radius R for a tangential deployment. The derived tether inertia for each case is included in later sections. The end of each tether is mounted with an end mass, also referred to as a payload mass, to enable centrifugal acceleration. The spacecraft is modeled with the additional mass of the stowed portion of the tethers placed along the circumference of the spacecraft. Combining the time varying stowed tether contribution of the inertia to the spacecraft, the inertia of the hub is expressed in the tether fixed $\mathscr{S}$ frame, where only the third axis term will be of a contributor to the planar deployment. This third axis term expressed in the tether frame is the same for all deployment models, where m_H is the hub mass.

$$I_{s_{33}} = \frac{1}{2}m_H R^2 + R^2(m_{T,0} - m_T) \qquad (3)$$

2.2. Equations of motion via Lagrange's equation

The equations of motion for each deployment concept are efficiently determined using the Lagrange energy based approach. The kinetic energy of the system is

$$T = T_H + \sum_{i=1}^{N} T_{T,i} + \sum_{i=1}^{N} T_{E,i} = T_H + T_T + T_E \qquad (4)$$

where subscript H refers to the spacecraft hub, T refers to the tethers, E refers to the tether end mass, and i indicates an individual tether or end mass. Assuming that all N tethers are deployed symmetrically at equal rates and have identical construction, these summation terms can be reduced to single lumped terms, where the energy contribution of the tether system is equivalent to a single tether of equivalent mass. Similarly, the energy contribution of the end masses is condensed. The kinetic energy of each component is then written as follows:

$$T_H = \frac{1}{2}\boldsymbol{\omega}_{\mathscr{B}/\mathscr{N}}^{\intercal}[I_s]\boldsymbol{\omega}_{\mathscr{B}/\mathscr{N}} \qquad (5a)$$

$$T_T = \frac{1}{2}\boldsymbol{\omega}_{\mathscr{S}/\mathscr{N}}^{\intercal}[I_T]\boldsymbol{\omega}_{\mathscr{S}/\mathscr{N}} + \frac{1}{2}m_T \dot{\boldsymbol{R}}_{T,C} \cdot \dot{\boldsymbol{R}}_{T,C} \qquad (5b)$$

$$T_E = \frac{1}{2}m_E \dot{\boldsymbol{R}}_E \cdot \dot{\boldsymbol{R}}_E \qquad (5c)$$

where the expressions of the inertias, velocities, and rotation rates are defined uniquely for the two cases in subsequent sections. The equations of motion are then derived using Lagrange's Equation, and are validated by checking for conservation of energy and angular momentum. Where there are no potential energy sources, this is simplified to

$$\frac{\mathrm{d}}{\mathrm{d}t}\left(\frac{\partial T}{\partial \dot{q}_j}\right) - \left(\frac{\partial T}{\partial q_j}\right) = Q_{nc_j} \qquad (6)$$

where the non-conservative force is the torque applied on the spacecraft hub. The contribution of this torque to each general coordinate equation is determined as follows.

$$Q_{nc_j} = \boldsymbol{u}_s \cdot \frac{\partial \boldsymbol{\omega}_{\mathscr{B}/\mathscr{N}}}{\partial \dot{q}_j} \qquad (7)$$

3. Tangential deployment method and parameter analysis

In this concept, the tethers are deployed tangentially using a free deployment, where the acceleration of the end mass advances the tether, much like with a yo-yo despinner. This concept is illustrated in Fig. 2, where the applied torque is represented with thrusters but could be achieved in other manners. Each of the tethers are wrapped about a central hub and are unreeled from the hub simultaneously. This method takes advantage of the spin stabilized system dynamics to actuate the deployment and relies only on the spacecraft spin rate. Therefore, control of the spacecraft spin rate will couple with the deployment rate, creating a more complex dynamical system but providing a free deployment scheme. Additionally, transitioning the fully deployed tangential tethers to a radial configuration must also be modeled. Therefore, the deployment is operated in two phases, an unwrap phase that releases the tether length, and a hinging phase that transitions the tethers from the tangential to radial configurations.

3.1. Equations of motion for tangential deployment

A dynamical model of the deployment is developed based on a spacecraft hub based control scheme. This model is primarily concerned with the momentum balance between the spacecraft hub, tethers, and tether end masses, and therefore makes several simplifying assumptions. The tethers and tether tip point-masses are assumed to behave in a symmetrical fashion, and therefore are described using one set of state parameters. The tether is treated as a time varying, straight slender rod and tether flexibility is not considered in this first order analysis. The parameters of this deployment method are defined in Fig. 3, which also includes the reference frame definitions, where the $\mathscr{S}$ frame is a tether-fixed frame, the $\mathscr{E}$ frame is a hub-fixed frame, and the $\mathscr{N}$ frame is inertial. Here ϕ is the deployment unwrap angle, measured from the tether tangent point's original position and ω is the spacecraft rate. Where the rotation rates with respect to the inertial frame are defined as

$$\boldsymbol{\omega}_{\mathscr{B}/\mathscr{N}} = \omega\widehat{\boldsymbol{s}}_3 \qquad (8)$$

$$\boldsymbol{\omega}_{\mathscr{S}/\mathscr{N}} = (\omega + \dot{\phi})\widehat{\boldsymbol{s}}_3 \qquad (9)$$

The velocity vectors are determined as

$$\dot{\boldsymbol{R}}_E = -R\omega\widehat{\boldsymbol{s}}_1 + R\phi(\omega + \dot{\phi})\widehat{\boldsymbol{s}}_2 \qquad (10)$$

$$\dot{\boldsymbol{R}}_{T,C} = -\frac{1}{2}R(2\omega + \dot{\phi})\widehat{\boldsymbol{s}}_1 + \frac{1}{2}R\phi(\omega + \dot{\phi})\widehat{\boldsymbol{s}}_2 \qquad (11)$$

Treating the inertia of the tether as a slender rod, and applying the parallel axis theorem, the inertia of the tethers with respect to an origin located at the spacecraft center of mass is shown in Eq. (12), expressed in the tether fixed $\mathscr{S}$ frame.
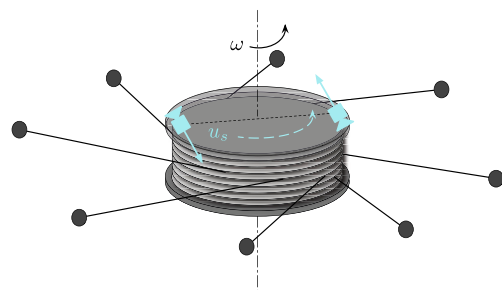

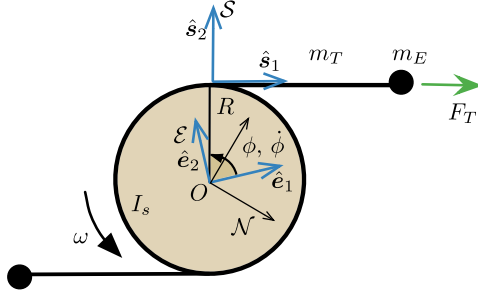**Fig. 2.** Concept diagram for the tangential deployment scheme.

Fig. 3. Tangential deployment dynamics parameters.

$$[I_T] = \begin{bmatrix} R^3\rho\phi & -\frac{1}{2}R^3\rho\phi^2 & 0 \\ -\frac{1}{2}R^3\rho\phi^2 & \frac{1}{3}R^3\rho\phi^3 & 0 \\ 0 & 0 & \frac{1}{12}R^3\rho\phi^3 + R\rho\phi\left(R^2 + \frac{1}{4}R^2\phi^2\right) \end{bmatrix} \quad (12)$$

These expressions are used to define the kinetic energy expressions of Eq. (5c). Then, the equations of motion are derived using Lagrange's Equation to be as follows. The spacecraft rate, ω, the tether unwrap angle, ϕ, and the unwrap rate, $\dot{\phi}$, are the state coordinates of this system. The hub applied torque is expressed as u_s.

$$\frac{1}{24}R^2\left(-3\left(4R\rho + 8m_E\phi + 7R\rho\phi^2\right)\omega^2 + 3\left(5R\rho + 8m_E\phi + 7R\rho\phi^2\right)\dot{\phi}\right) +$$
$$\frac{1}{12}R^2\phi\left(18R\rho + 12m_E\phi + 7R\rho\phi^2\right)\dot{\omega} + \frac{1}{12}R^2\phi\left(15R\rho + 12m_E\phi + 7R\rho\phi^2\right)\ddot{\phi} = 0$$
$$(13)$$

$$\frac{1}{12}R^2\left(3\left(4R\rho + 8m_E\phi + 7R\rho\phi^2\right)\omega\dot{\phi} + 3\left(6R\rho + 8m_E\phi + 7R\rho\phi^2\right)\dot{\phi}^2\right) +$$
$$\frac{1}{12}R^2\left(6\left(2m_E + m_H + 2m_{T,0}\right) + 12R\rho\phi + 12m_E\phi^2 + 7R\rho\phi^3\right)\dot{\omega} +$$
$$\frac{1}{12}R^2\phi\left(18R\rho + 12m_E\phi + 7R\rho\phi^2\right)\ddot{\phi} = u_s \quad (14)$$

This model only applies to the point where the tethers are fully unwrapped. Following this point, the tethers must transition to a radial orientation with respect to the hub, and this transition will be referred to as the hinging phase. Using similar methods as those described above, the hinge phase equations of motion are also determined. The parameters of interest are defined in Fig. 4. The tether has freedom to rotate about the connection point by angle β, where the desired dynamics will come to rest at $\beta = 90$deg. The deployment angle ϕ is now fixed constant. The angular rate and velocities of the end mass and the tether center of mass are now described in the $\mathscr{S}$ frame.

$$\boldsymbol{\omega}_{\mathscr{S}/\mathscr{N}} = \left(\omega + \dot{\beta}\right)\widehat{\boldsymbol{s}}_3 \quad (15)$$
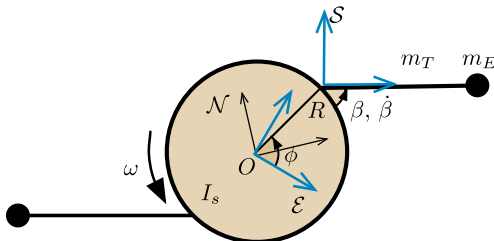
Fig. 4. Hinging from tangential to radial dynamics parameters.

$$\dot{\boldsymbol{R}}_{E,H} = R\dot{\phi}\widehat{\boldsymbol{s}}_1 \quad (16)$$

$$\dot{\boldsymbol{R}}_{T,H} = -R\cos\beta\omega\widehat{\boldsymbol{s}}_1 + \frac{1}{2}R\left((\phi + 2\sin\beta)\omega + \phi\dot{\beta}\right)\widehat{\boldsymbol{s}}_2 \quad (17)$$

The tether inertia for this phase is determined where the hinging position description is used. Only the third axis inertia is required in the planar dynamics.

$$I_{T,H_{33}} = \frac{1}{3}R^3\rho\phi\left(3 + \phi^2 + 3\phi\sin\beta\right) \quad (18)$$

These expressions define the kinetic energy state of the system expressed in Eq. (5c), and the Lagrange equations can now be used to determine the equations of motion for the hinging phase.

$$\frac{1}{2}R^2\phi\cos\beta\left(-2(m_E + R\rho\phi)\omega^2 + R\rho\phi\dot{\beta}^2\right) +$$
$$\frac{1}{12}R^2\phi\left(12m_E\phi + R\rho\left(12 + 7\phi^2\right) + 6(2m_E + 3R\rho\phi)\sin\beta\right)\dot{\omega} +$$
$$\frac{1}{12}R^2\phi\left(12m_E\phi + R\rho\left(12 + 7\phi^2\right) + 12R\rho\phi\sin\beta\right)\ddot{\beta} = 0 \quad (19)$$

$$\frac{1}{12}R^2\left(24\phi(m_E + R\rho\phi)\cos\beta\omega\dot{\beta} + 6\phi(2m_E + 3R\rho\phi)\cos\beta\dot{\beta}^2\right) +$$
$$\frac{1}{12}R^2\left(6m_H + 12m_{T,0} + 12m_E\left(1 + \phi^2\right) + R\rho\phi\left(12 + 7\phi^2\right) + 24\rho(m_E + R\rho\phi)\sin\beta\right)\dot{\omega} +$$
$$\frac{1}{12}R^2\phi\left(12m_E\phi + R\rho\left(12 + 7\phi^2\right) + 6(2m_E + 3R\rho\phi)\sin\beta\right)\ddot{\beta} = u_s \quad (20)$$

3.2. Constant spacecraft rate in tangential deployment

The deployment behavior is strongly influenced by the reference rate maintained by the spacecraft. A constant spacecraft rate is the simplest to implement and will be analyzed in detail here to provide a baseline case. The constant rate case is further valuable in that it provides insights into the deployment parameter relationships and behaviors. Additionally, it may be desirable in that it provides a predetermined reference trajectory and enables prediction of system behavior. Alternative objectives, such as tracking to maintain a constant tether tension, require live self observations and live updates of the reference trajectory, however in subsequent sections it is shown that these time varying cases will improve deployment time significantly. Looking at the tether tension expression:

$$\boldsymbol{T} = m_{E_i}R\left(\phi\left(\omega + \dot{\phi}\right)^2 + \dot{\omega}\right)\widehat{\boldsymbol{s}}_1 + m_{E_i}R\left(\omega^2 - \dot{\phi}^2 - \phi(\dot{\omega} + \ddot{\phi})\right)\widehat{\boldsymbol{s}}_2 \quad (21)$$

where there is no tension in the $\widehat{\boldsymbol{s}}_\phi$ direction, this portion of the expression can be set equal to zero. For a constant spacecraft rate, assuming the tether deployment is not accelerating, this expression can be used to prove that the deployment rate with respect to the spacecraft will be equal to the spacecraft spin rate

$$\omega = \dot{\phi} \quad (22)$$

and this is observed in the numerical simulations shown in Fig. 6. Further applying these assumptions to the tension expression, the tether tension at a given point in the deployment is determined for an individual tether, i, from:

$$T = 4m_{E_i}\omega^2 R\phi \quad (23)$$

Additionally, assuming perfect tracking and constant rates, the torque required through the deployment duration is derived from the equations of motion to be

$$u_s = \frac{1}{12}R^2\left(30R\rho + 48m_E\phi + 42R\rho\phi^2\right)\omega^2$$

It is notable that the tension and torque do not rely on the spacecraft mass. These relationships can then be used to explore the sensitivity of the system to E-sail parameter choices. Of particular interest is the effect of the payload mass size on the rate requirements and deployment time. Where the maximum allowable tension in the proposed Hoytether is known to be 0.05 N, the maximum allowable spin rate can be determined

$$\omega_{\max} = \sqrt{\frac{T_{\max}}{4m_{E_i}R\phi_f}} \tag{24}$$

where ϕ_f is the final ϕ after deployment. These expressions show that the deployment tension and rate restrictions are only a function of the end mass and tether length, and other parameters, such as the spacecraft mass and tether mass, are not influential. Maps of these expressions as a function of the tether length, which can be determined from the deployment angle, and the payload end mass are displayed in Fig. 5. These plots quickly demonstrate that for the constant spacecraft rate case, where the tension increases linearly over time and the maximum tension will be reached at the end of the deployment, the deployment requires long deployment times for large end mass payloads. One primary advantage of the E-sail propulsion in comparison to others is the relatively fast outer planet trajectory cruise times, which are on the order of 6–10 years for outer solar system destinations. If the sail requires nearly a year to deploy it will greatly impact the spacecraft acceleration and trajectory. Where the acceleration is most effective closer to the Sun, the E-sail deployment will most likely occur during the most propulsion-effective period of the trajectory (the exception being a case where the

deployment is executed as the spacecraft ballistically approaches an inner planet flyby). This strongly motivates searching for time minimal deployment schemes that will reduce the impact on the E-sail effectiveness. Additionally, for smaller payloads, the torque required to reach the desired tension is well outside the range of feasible torque capabilities for modern spacecraft. This strongly motivates investigation of time-varying reference rate trajectories that will minimize deployment time while not exceeding torque capabilities.

3.3. Hub rate tracking feedback control analysis

Lyapunov stability theory provides an analytical method to evaluate and develop controlled nonlinear dynamical systems using stability definitions and Lyapunov functions [21]. Using this method, a feedback control is developed that proves the hub-actuated, spacecraft-rate focused controller will be applicable and stable for this system. A positive definite Lyapunov function is chosen for this development and is defined in (25). It is desired that the spacecraft rate is controlled by a hub applied torque and tracks to a reference trajectory. Therefore, the Lyapunov function is only a function of the tracking error, $\delta\omega = \omega - \omega_r$.

$$V(\delta\omega) = \frac{\delta\omega^2}{2} \tag{25}$$

The time derivative of the Lyapunov function is now taken:

$$\dot{V}(\delta\omega) = \delta\omega\delta\dot{\omega} \tag{26}$$

(a) max allowable body rate (deg/s)
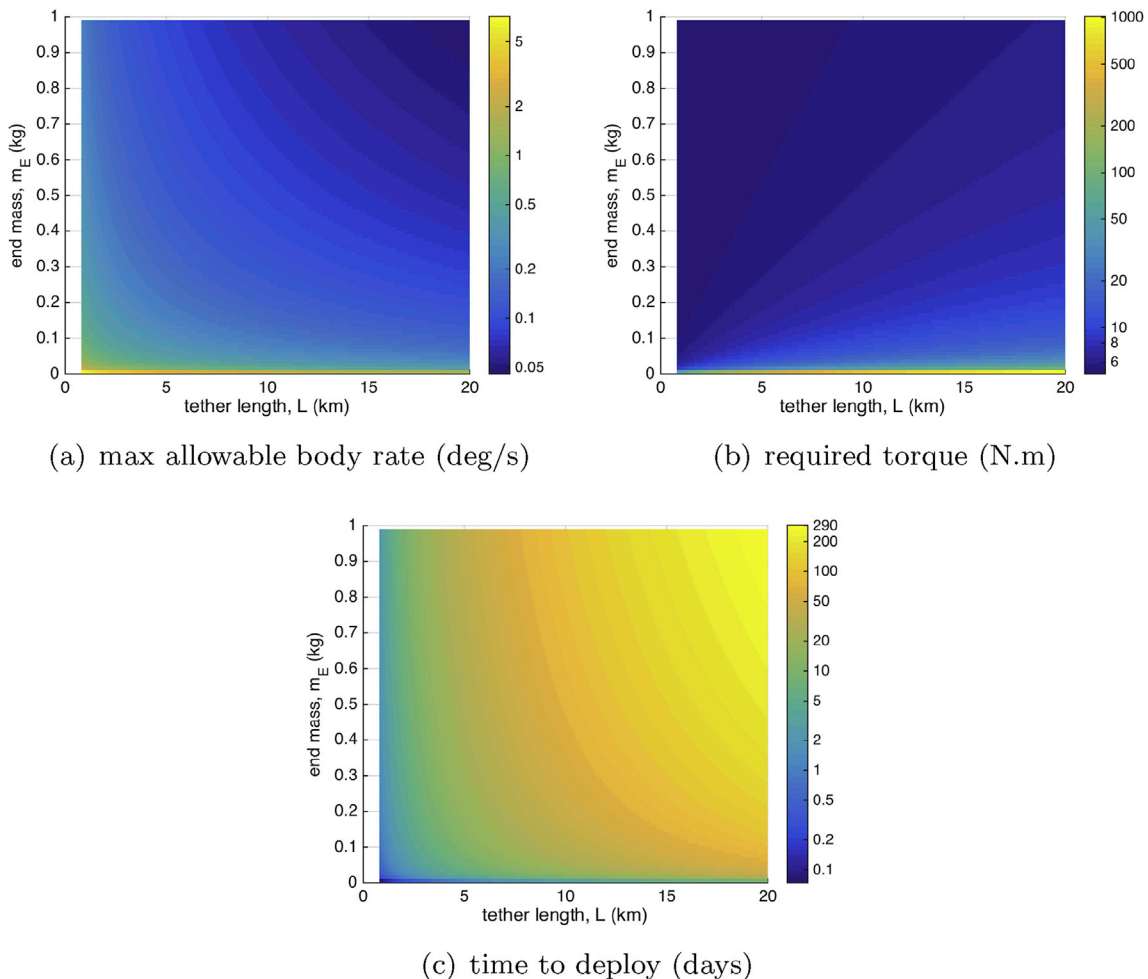
(b) required torque (N.m)

(c) time to deploy (days)

Fig. 5. Color maps of the maximum allowable spacecraft body rate and the corresponding torque required to maintain that rate and the time to deploy for the constant body rate case. (For interpretation of the references to colour in this figure legend, the reader is referred to the Web version of this article.)

To have asymptotic stability, the time derivative of the Lyapunov function must be negative definite. To find a control that guarantees this, (26) is set equal to a negative definite Lyapunov rate expression.

$$\dot{V}(\delta\omega) = -P\delta\omega^2 = \delta\omega\delta\dot{\omega} \tag{27}$$

Simplifying yields:

$$-P\delta\omega = \delta\dot{\omega} = \dot{\omega} - \dot{\omega}_r \tag{28}$$

where P is a positive gain. To determine the control torque, the expression for $\dot{\omega}$ as a function of torque, u_s, is substituted into Eq. (14) and u_s is solved for, shown in (29).

$$u_s = \frac{1}{24}R^2\left(-3\left(4R\rho + 8m_E\phi + 7R\rho\phi^2\right)\omega^2 + 3\left(5R\rho + 8m_E\phi + 7R\rho\phi^2\right)\dot{\phi}\right) +$$
$$+\frac{1}{12}R^2\phi\left(15R\rho + 12m_E\phi + 7R\rho\phi^2\right)\ddot{\phi} - P\frac{1}{12}R^2\phi\left(18R\rho + 12m_E\phi + 7R\rho\phi^2\right)\delta\omega \tag{29}$$

3.4. Spacecraft rate trajectory for tension maintenance

Alternatively, the spacecraft rate trajectory can be derived such that the tension is maintained constant. This allows for a time-minimum deployment, where the strength of material is treated as the limiting factor. To determine this reference rate, the time derivative of the tension expression is set equal to zero:

$$\dot{T} = m_{E_i}R\left(\dot{\phi}(\omega + \dot{\phi})^2 + 2\phi(\omega + \dot{\phi})(\dot{\omega} + \ddot{\phi}) + \ddot{\omega} = 0\right) \tag{30}$$

Assuming there is no jerk, $\ddot{\omega} = 0$, the relationship between the spacecraft rate and the deployment rate is determined as

$$\dot{\phi} = 2\omega \tag{31}$$

substituting this into Eq. (30), the spacecraft rate required to provide constant tension as a function of deployment angle is

$$\omega^2 = \frac{T_{max}}{m_{E_i}R\left(9\phi - \frac{1}{\phi}\right)} \tag{32}$$

The expression above cannot be used alone as a reference, where the expression is not defined for $\phi = 0$ and would exceed allowable rates for small ϕ. Therefore, a maximum allowable rate must be identified for the spacecraft and applied for the initial trajectory as a part of a piecewise approach, defined in Eq. (33). For simulation purposes, the maximum allowable spacecraft spin rate is set to 2.5 deg/s. The behavior for a deployment case where this is used as the reference speed is now compared to the constant rate case. Fig. 6 shows the behavior over time for these two cases, where the E-sail size parameters are chosen such that the characteristic acceleration is 0.1 mm/s² and there are 20 tethers, determining the tether length to be 4.3 km. The payload mass is set to a modest 50 g to represent a dummy mass or independent sensor device. These and other relevant parameters are listed in Table 1.
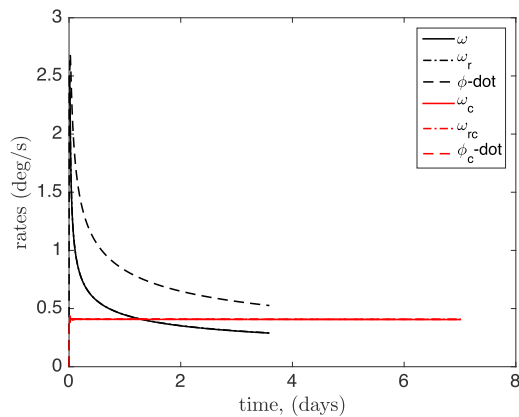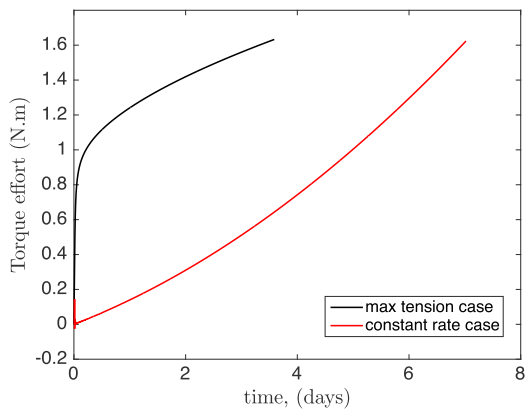

(a) body and tether rates
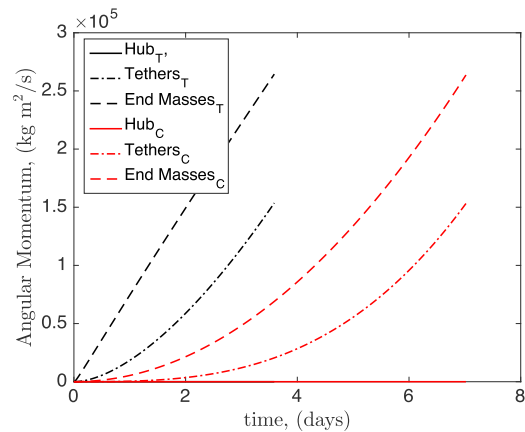
(b) angular momentum of each component
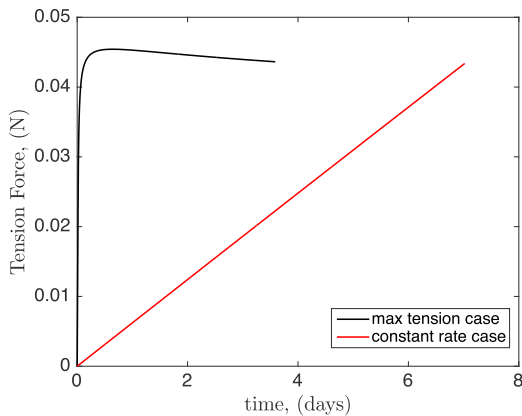
(c) tension force in each tether

(d) torque required

Fig. 6. Unwrap phase deployment of the tangentially deployed E-sail with a constant reference trajectory (black) and a tension derived trajectory (red). (For interpretation of the references to colour in this figure legend, the reader is referred to the Web version of this article.)

Table 1
Spacecraft and E-sail parameters implemented in example simulations.

$a_\oplus$ mm/s^2	N	L km	m_{E_i} kg	m_T kg	m_H kg
0.1	20	4.3	0.050	0.996	500

$$\omega = \begin{cases} \omega_{\text{const}} & \omega_{\text{non-lin}} \geq \omega_{\text{max}} \\ \omega_{\text{non-lin}} & \omega_{\text{non-lin}} \leq \omega_{\text{max}} \end{cases} \tag{33}$$

3.5. Numerical simulations

The tension optimized reference trajectory is shown to decrease the deployment time from 7.02 days to 3.59 days, or to 51% of the constant rate deployment time. This is somewhat consistent with the expressions of expected deployment rate, Eq. (22) and Eq. (31), which predict the tension derived reference will deploy at twice the hub rate. This is a notable savings and will be instrumental for deployment design, where the greatest strength of this concept is it's potential for implementing fast missions to the outer solar system and any time lost during deployment may detract from that. The tensions achieved at the end of the deployment are within 0.5% of each other, providing nearly equivalent end-tension cases. It is notable that the maximum torque capability needed to achieve the deployment is the same for

$$\frac{1}{12}\left(6R\rho\sin\beta\dot{l}^2 - 12Rl\sin\beta m_E\dot{\beta}(\dot{\beta} + 2\omega) - 6R\rho l^2\sin\beta\dot{\beta}(3\dot{\beta} + 4\omega)\right)$$
$$+\frac{1}{12}\left(3\dot{i}\left((4R^2\rho + 7\rho l^2 + 8lm_E)(\dot{\beta} + \omega) + 2R\cos\beta(4m_E(\dot{\beta} + \omega) + \rho l(7\dot{\beta} + 8\omega))\right)\right)+$$
$$\frac{1}{12}\left(12R^2\rho l + 24R\rho\cos\beta l^2 + 7\rho l^3 + 24R\cos\beta lm_E + 12l^2 m_E + 6R^2(2m_E + m_H + 2m_{T,0})\right)\dot{\omega}+$$
$$\frac{1}{12}\left(12R^2\rho l + 18R\rho\cos\beta l^2 + 7\rho l^3 + 12R\cos\beta lm_E + 12l^2 m_E\right)\ddot{\beta} = u_s \tag{38}$$

both cases, however the maximum tension case has a higher average torque over the shorter duration. The hinge phase of both deployments are shown in Fig. 7, and it's noted that the two cases have nearly identical hinging behaviors. Although there is a difference in the spacecraft rates at the start of deployment, at the moment hinging begins, the tether deployment rates, $\dot{\phi}$, are transferred to tether hinging rates, and the net behavior is the same. The applied torque ramps down as the tethers decelerate and transfer to the desired position and the hinging is completed smoothly in under 15 min. This shows that controlled hinging can be accomplished using the hub-mounted control scheme.

4. Radial modeling and parameter analysis

Another method to deploy the E-sail is to use radially deploying tethers, as seen in Fig. 8. Such a design requires tether reeling modules to stow and control each of the 20–100 tethers individually, and therefore requires 20–100 drive mechanisms. This introduces a large power consumption during the deployment as well as synchronization challenges. Additionally, the system still experiences significant momentum exchange and rate changes that couples with the unreeling process. However, this method enables highly valuable independent control of the tethers and decouples deployment failure risks of the tethers from each other. Furthermore, substantial engineering development has been done on a reeling mechanism [13]. Energy methods are used to determine the equations of motion for the radial deployment case.

4.1. Radial deployment equations of motion

A dynamics model of this concept is developed using the simplified schematic illustrated in Fig. 9. Here β is the angle of deviation of the tether from radial, and $\dot{\beta}$ is the rotation rate of the tether. The tether rotation with respect to inertial is

$$\boldsymbol{\omega}_{\mathscr{S}/\mathscr{N}} = (\omega + \dot{\beta})\hat{\boldsymbol{s}}_3 \tag{34}$$

Then the velocity vectors are described in the $\mathscr{S}$ frame as

$$\dot{\boldsymbol{R}}_{E,H} = \left(\dot{l} + R\sin\beta\omega\right)\hat{\boldsymbol{s}}_1 + \left(l(\dot{\beta} + \omega) + R\cos\beta\omega\right)\hat{\boldsymbol{s}}_2 \tag{35}$$

$$\dot{\boldsymbol{R}}_{T,H} = \left(\frac{1}{2}\dot{l} + R\sin\beta\omega\right)\hat{\boldsymbol{s}}_1 + \left(\frac{1}{2}l(\dot{\beta} + \omega) + R\cos\beta\omega\right)\hat{\boldsymbol{s}}_2 \tag{36}$$

The radial tether inertia of the third axis is determined to be:

$$I_{T,H_{33}} = \frac{1}{12}\rho l^3 + \rho l\left(\left(R\cos\beta + \frac{1}{2}l\right)^2 + R^2\sin\beta^2\right) \tag{37}$$

Using these definitions for the model components, the energy of the system is determined using Eq. (4). Using again the Lagrangian dynamics formulation, the coupled equations of motion for the hub rate ω and deflection angle β are

$$\frac{1}{12}\left(6Rl\sin\beta\left(-\rho l\dot{\beta}^2 + 2(\rho l + m_E)\omega^2\right)\right)+$$
$$\frac{1}{12}\left(3\dot{i}\left((4R^2\rho + 7\rho l^2 + 8lm_E)(\dot{\beta} + \omega) + 2R\rho\cos\beta l(4\dot{\beta} + 5\omega)\right)\right)+$$
$$\frac{1}{12}\left(6R\cos\beta l(3\rho l + 2m_E) + l(12R^2\rho + 7\rho l^2 + 12lm_E)\right)\dot{\omega}+$$
$$\frac{1}{12}\left(12R\rho\cos\beta l^2 + l(12R^2\rho + 7\rho l^2 + 12lm_E)\right)\ddot{\beta} = 0 \tag{39}$$

4.2. Radial deployment with constant spacecraft rate case

Similarly to the tangential model analysis, the constant hub rate case can be further analyzed for the radial model. However unlike the tangential case, the deployment rate of the radial case is controlled by $\dot{l}$ which is assumed to be controlled by the spool motor and held constant. Therefore, adjustments in the reference rate will not result in a time savings. While including the deployment rate as a free variable is possible, it adds significant complexity to the model and is left for future work. For a radial orientation, the tether tension is written as

$$\boldsymbol{T} = m_{E_i}\left(R\cos\beta\omega^2 + l(\dot{\beta} + \omega)^2\right)\hat{\boldsymbol{s}}_R - m_{E_i}\left(R\sin\beta\omega^2 + 2\dot{l}(\dot{\beta} + \omega) + l\ddot{\beta}\right)\hat{\boldsymbol{s}}_\phi \tag{40}$$

(a) body and tether rates

(b) tether hinge rate

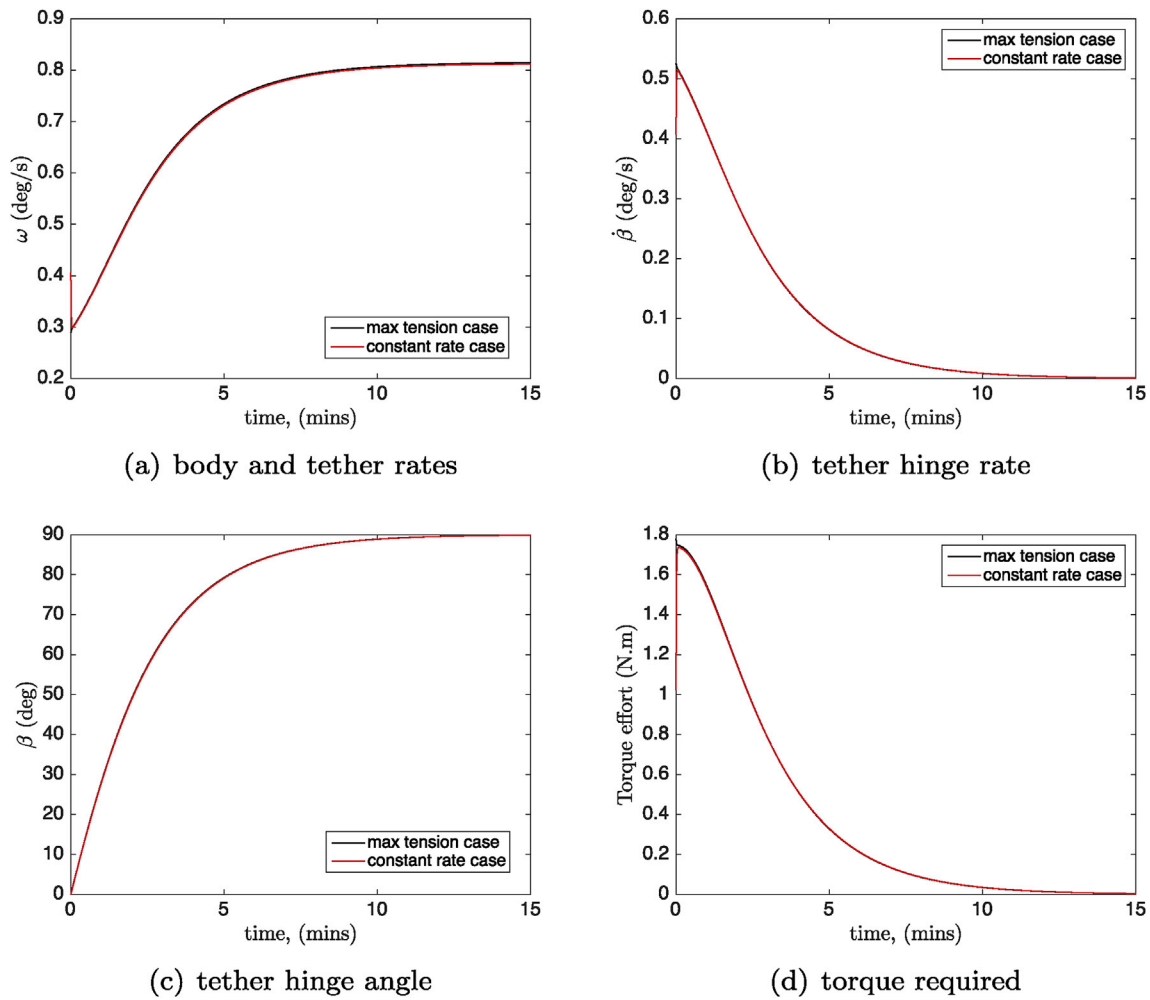
(c) tether hinge angle

(d) torque required

Fig. 7. The hinge phase of the tangentially deployed E-sail is shown to be the same for a constant reference trajectory (black) and a tension derived trajectory (red). (For interpretation of the references to colour in this figure legend, the reader is referred to the Web version of this article.)
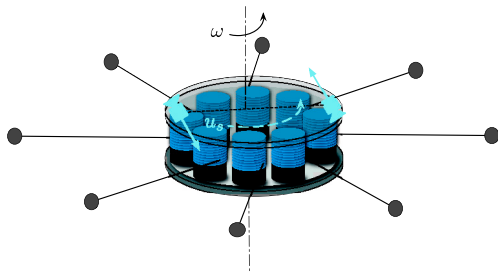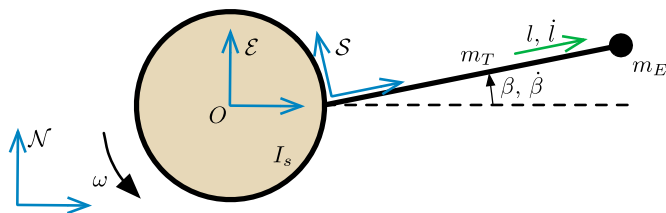

Fig. 8. Concept diagram of the radial deployment scheme.

Fig. 9. Radial deployment dynamics parameters.

where there is no tension in $\widehat{s}_\phi$, the tether normal direction, the following are known:

$$T = m_{E_i}\left(R\cos\beta\omega^2 + l\left(\dot{\beta} + \omega\right)^2\right) \tag{41}$$

$$-m_{E_i}\left(R\sin\beta\omega^2 + 2\dot{l}\left(\dot{\beta} + \omega\right) + l\ddot{\beta}\right) \tag{42}$$

Assuming the tether's position is not changing or accelerating, $\dot{\beta} = 0$ and $\ddot{\beta} = 0$, Eq. (42) is used to solve for an expression of β:

$$\beta = \sin^{-1}\frac{-2\dot{l}}{R\omega} \tag{43}$$

This result proves that for a radially deploying spin stabilized tether, there must be some deviation from the radial orientation during deployment. This is a significant result that implies a trade between the deployment rate, spacecraft rate, and tether position deviation. Due to the assumptions made in the derivation, there is some deviation from the predicted position and the observed position in numerical simulations. However, the prediction is within 2% accuracy. Furthermore, by this definition, the quantity including the ratio of the linear deployment rate to the spacecraft rate must be from 0 to 1 for the tether position to be defined. This limits the possible rate configuration of the system.

4.3. Lyapunov control stability analysis

Similarly to the tangential case, the Lyapunov function for the radial deployment is only a function of the tracking error, $\delta\omega = \omega - \omega_r$, and the same Lyapunov function and derivation methods are applied here. To

determine the control torque, the expression for $\dot{\omega}$ as a function of torque, u_s, is substituted into Eq. (38) and u_s is solved for. This derivation assumes a constant reference rate.

there is a factor of 2 in the constant expression and a factor of 3/2 here, indicating that this reference trajectory maintains a smaller tension deviation than the constant case. The spin rate trajectory corresponding

$$u_s = \frac{1}{12}\left(6R\rho\sin\beta\dot{l}^2 - 12Rl\sin\beta m_E\dot{\beta}(\dot{\beta}+2\omega) - 6R\rho l^2\sin\beta\dot{\beta}(3\dot{\beta}+4\omega)\right)+$$

$$\frac{1}{12}\left(3\dot{l}\left(\left(4R^2\rho + 7\rho l^2 + 8lm_E\right)(\dot{\beta}+\omega) + 2R\cos\beta\left(4m_E(\dot{\beta}+\omega) + \rho l(7\dot{\beta}+8\omega)\right)\right)\right)+$$

$$\frac{1}{12}\left(12R^2\rho l + 18R\rho\cos\beta l^2 + 7\rho l^3 + 12R\cos\beta lm_E + 12l^2m_E\right)\ddot{\beta} - P\frac{1}{12}\left(12R^2\rho l + 24R\rho\cos\beta l^2 + 7\rho l^3 + 24R\cos\beta lm_E + 12l^2m_E + 6R^2(2m_E + m_H + 2m_{T,0})\right)\delta\omega$$

$$(44)$$

4.4. Spacecraft rate trajectory for tension maintenance

Considering instead the time-minimum approach where the tension force in the tether is maximized and maintained constant, assuming the tether's position is not changing or accelerating, and that there is no jerk on the spacecraft hub, the position of the tether can be predicted as

$$\beta = \sin^{-1}\frac{-3\dot{l}}{2R\omega} \tag{45}$$

Which is similar to what is determined for the constant rate case, where

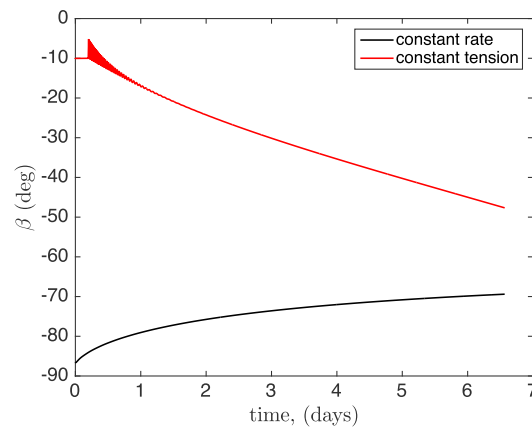with this is determined as a function of the current tether deployment length and rate as

$$\omega = \sqrt{\frac{8T_{\max}(2\rho L + m_{E_i}) + \rho m_{E_i}\dot{l}^2}{m_{E_i}(4R^2\rho + 23\rho l^2 + 16lm_{E_i})}} \tag{46}$$
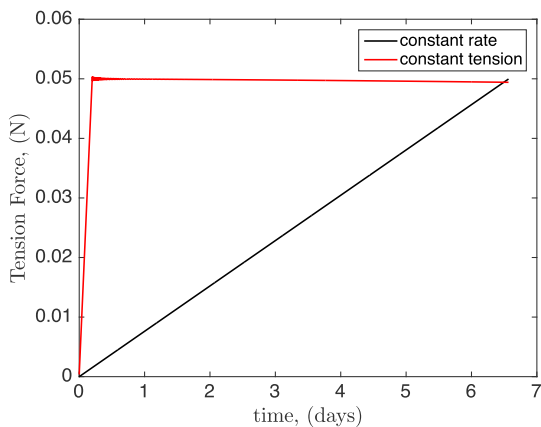
4.5. Numerical simulation

The response of the system to this reference trajectory is illustrated in Fig. 10 along with the constant rate case. The deployment rate, $\dot{l}$, in both
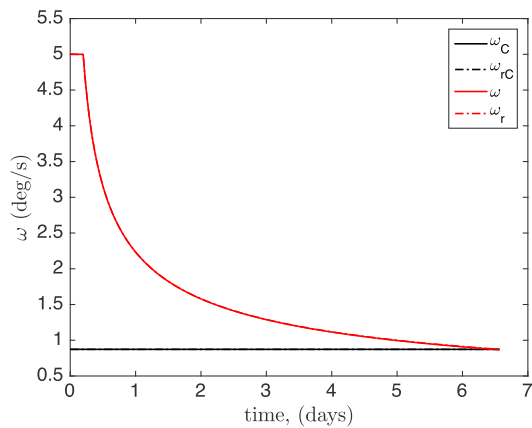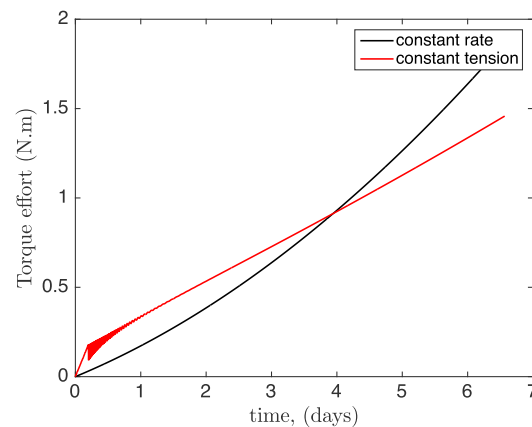

(a) body and tether rates

(b) tether hinge angle

(c) tension force in each tether

(d) torque required

Fig. 10. Behaviors of the radially deployed E-sail with a constant reference trajectory (black) and a tension derived trajectory (red). (For interpretation of the references to colour in this figure legend, the reader is referred to the Web version of this article.)
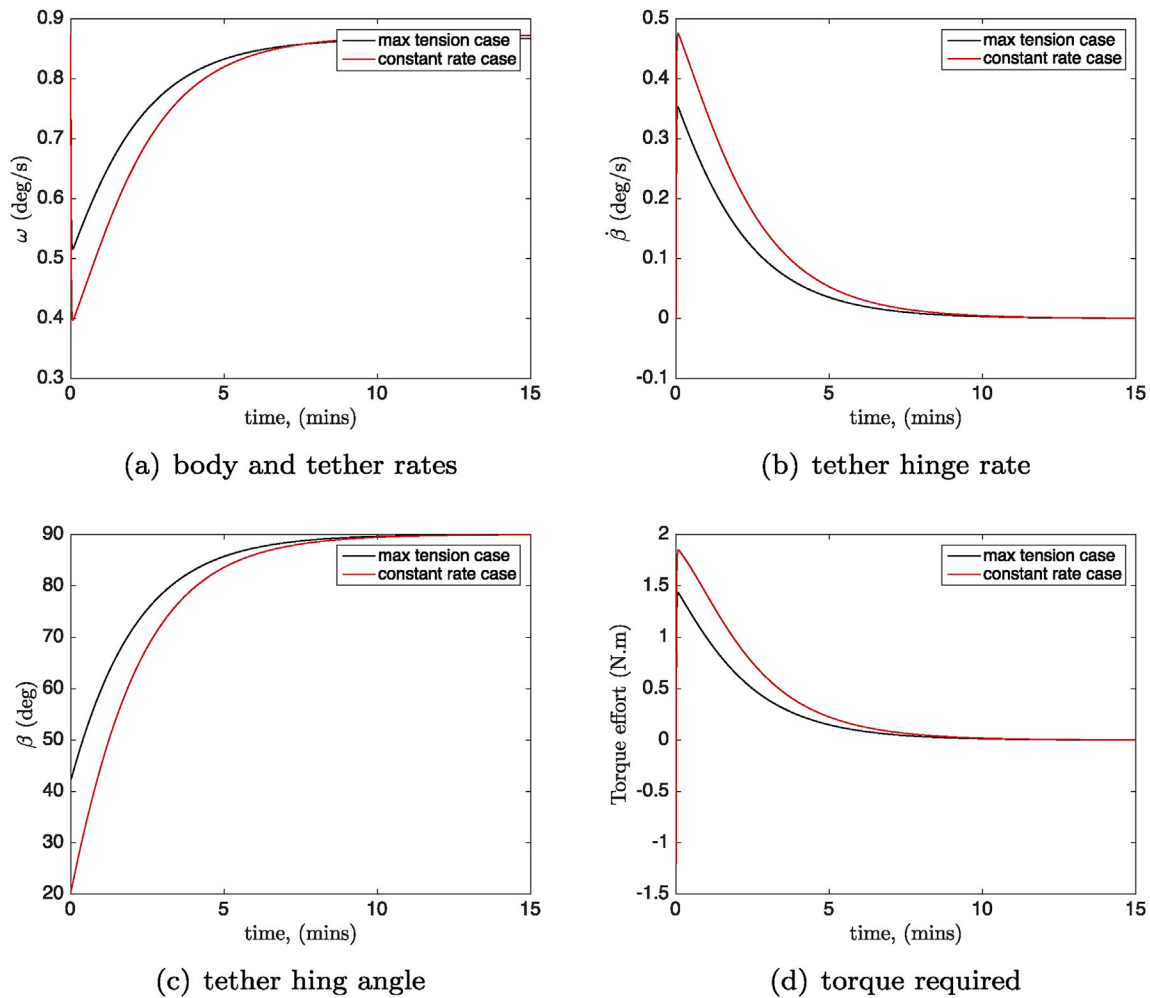
(a) body and tether rates

(b) tether hinge rate

(c) tether hing angle

(d) torque required

Fig. 11. The hinging phases of the radially deployed E-sail deployment with a constant reference trajectory (black) and a tension derived trajectory (red) are slightly different due to the difference in initial tether angle. (For interpretation of the references to colour in this figure legend, the reader is referred to the Web version of this article.)

cases is equivalent and constant, however, so the time to deploy is equivalent. However, the tether angle in the time varying trajectory is notably smaller, and the magnitude of the torque effort required is smaller, despite maintaining a higher tension. This analysis does not account for the additional spin up phase prior to deployment which is assumed to be provided by the launch vehicle stages. The discontinuity in the position angle occurs at the switch of the piecewise reference trajectory, and is attributed to the derived expressions of the tether position angle for the two cases. Eq. (45) and Eq. (43) show that the predicted tether position will change, and the numerical simulation reflects this discontinuity. As in the tangential case, due to the tether position displacement, a hinging maneuver will need to be executed at the end of the deployment. Fig. 11 illustrates the hinging for these two cases. The constant rate case, which has more displacement from radial, is shown to require a slightly more time and a greater torque effort to complete the transition, but overall these two cases show similar behavior.

5. Torque feasibility

One important question to address is how feasible the torque requirements are. The deployment torque can be applied to the hub using a variety of methods, depending on the order of magnitude and duration of torque needed for the deployment. Electric thrusters may be ideal candidates for their range of thrust magnitudes and time varying capabilities. Reaction wheels could also be used if fine control is needed, however the momentum stored in the wheels would need to

be actively removed. Chemical thrusters may also be used to achieve large torques for large E-sails, however the time variations could only be achieved using pulse width modulation thrust. The effects of such an approach on the deployment dynamics must be investigated to ensure stability. The mass of propellant needed for the electric or chemical thruster options is a primary concern for feasibility. Knowing the torque required as a function of time, the force provided at a given radius from the spin axis is easily determined. Using Eq. (47), which assumes a constant force and relates the propellant mass to the I_{sp} and force, the mass needed for each instant in time is found and numerically integrated over time. The constant force expression is used as a rough estimation, where including full time varying force presents a greater challenge than required.

$$\dot{m}_p = \frac{F_T}{g I_{sp}} \tag{47}$$

Assuming the thrusters are placed at a 1 m radius on the spacecraft and an electric thruster $I_{sp} = 2000$ s, and considering the tangential case presented earlier, the propellant mass for this example sail is $m_p =$ 21 kg for either constant rate or constant tension case. The previously proposed mass budget allocates 1 kg for each tether thruster unit, and therefore for the 20 tether case, the thruster mass described above is comparable. Recognizing that the example sail shown here provides small characteristic acceleration and larger sails will be desired, the propellant needed to deploy a large sail was investigated and will be hundreds of kilograms of propellant mass if a 1 m radius is used. This

is significant mass, however, it can be quickly reduced if larger moment arms are considered. Where the spacecraft hub might not exceed 1–2 m, the thrusters could possibly be mounted on deployable booms to increase the moment arm to achieve more efficient torque. Using 10 m booms, the propellant mass would then be on the order of 10's of kilograms, achieving considerable mass savings. A final point to address is again the idea of placing thrusters on the tether tips to provide torque. While this configuration does provide the best moment arm, the mass efficiency of these thrusters depends entirely on the I_{sp}, and locating the units at the tether tips restricts these to be independently functioning thrusters, and the design of such units may not be capable of achieving high I_{sp}. Additionally, the flexible dynamics of tether tip-mounted thrust would need to be investigated to ensure the concept behaves as desired.

6. Conclusions and future work

The two E-sail deployment schemes investigated in this paper provide feasible means to actuate the deployment of an E-sail structure using hub mounted torque only. The tangential deployment scheme provides a simpler deployment for lower torque, however it removes the ability to control the individual tether spooling. Deployment in a truly radial configuration, where $\beta \approx 0$, is shown to require much greater spin rates or much longer deployment duration than the case where tethers are allowed to drift, and reasonable deployment and spacecraft rates must have position drift. The advantage of an ideal radial deployment is that a hinge phase would not be needed, however in practical application, hinging will greatly reduce the deployment time or hub spin rate requirements and will be needed. The spacecraft rate trajectory, deployment rate, characteristic acceleration, and tether tip mass are large contributors to the deployment dynamics and must be chosen judiciously. Defining realistic boundaries for these parameters based on technology capabilities and mission requirements will inform future simulations. Additionally, it is noted that E-sails designed to have a greater number of shorter tethers have smaller inertia and therefore require less energy and momentum to deploy. However, these tethers would be in closer proximity to each other and may present collision risks. State error estimation of the tether positions must be done to determine the closest allowable proximity of two adjacent tethers. Future work will model each tether individually with a unique state and determine the factors influencing variation in position to do this. An additional concern is that the flexible tethers may exhibit in-plane bending despite internal tension. Model fidelity will therefore be further increased by using a lumped-mass method to incorporate the flexibility of the tethers. While many questions on the finer behavior of the E-sail deployment remain, the baseline momentum and torque requirements of the hub actuated deployment are now defined.

References

[1] P. Janhunen, Electric sail for spacecraft propulsion, J. Propul. Power 20 (4) (2004) 763–764.

[2] P. Janhunen, The electric sail - a new propulsion method which may enable fast missions to the outer solar system, J. Br. Interplanet. Soc. 61 (8) (2008) 326–329.

[3] P. Janhunen, A. Sandroos, Simulation study of solar wind push on a charged wire: basis of solar wind electric sail propulsion, Ann. Geophys. 25 (2007) 755–767.

[4] L. Johnson, R.M. Young, E.E. Montgomery IV, Status of solar sail propulsion: moving toward an interstellar probe, AIP Conf. Proc. 886 (2007) 207–214.

[5] P. Janhunen, J. Lebreton, S. Merikallio, Fast e-sail uranus entry probe mission, Planet. Space Sci. 104 (2014) 141–146.

[6] A.A. Quarta, G. Mengali, Electric sail missions to potentially hazardous asteroids, Acta Astronaut. 66 (2010) 1506–1619.

[7] G. Mengali, A.A. Quarta, Electric sail performance analysis, J. Spacecraft Rockets 45 (1) (2008) 122–129.

[8] P. Janhunen, Physics of thrust prediction of the solar wind electric sail propulsion system, in: N.V. Pogorelov, E. Audit, G.P. Zank (Eds.), Numerical Modeling of Space Plasma Flows, Astronum-2009, Vol. 429 of Astronomical Society of the Pacific Conference Series, 2010, p. 187.

[9] P. Toivanen, P. Janhunen, Thrust vectoring of an electric solar wind sail with a realistic sail shape, Acta Astronaut. 131 (2017) 145–151.

[10] P. Janhunen, P. Toivanen, Ti tether Rig for Solving Secular Spinrate Change Problem of Electric Sail, Aerospace Science and Technology.

[11] R. Hoyt, R.L. Forward, The hoytether: a failsafe multiline space tether structure, Sci. Tech. Aero. Rep. 36 (1998) 369–378.

[12] H. Seppänen, T. Rauhala, S. Kiprich, J. Ukkonen, M. Simonsson, R. Kurppa, P. Janhunen, E. Hæggström, One kilometer (1 km) electric solar wind sail tether produced automatically, Rev. Sci. Instrum. 84 (9) (2013) 095102–095106.

[13] R. Rosta, O. Kromer, T. Zoest, P. Janhunen, Wrecker: an unreeling mechanism for a thin electrically conductive space tether, CEAS Space J. 7 (2015) 53–68.

[14] A. Slavinskis, et al., Estcube-1 in-orbit experience and lessons learned, Aerosp. Electron. System. Mag. IEEE 30 (2015) 12–22.

[15] M.L. Cosmo, E.C. Lorenzini, Tethers in Space Handbook, third ed., Smithsonian Astrophysical Observatory, Cambridge, Massachusetts, 1997.

[16] D.A. Quinn, D.C. Folta, A tethered formation flying concept for the specs mission, in: 23rd Annual AAS Guidance and Control Conference, vol. 38, American Astronautical Society, Breckenridge, CO, 2000.

[17] U.J. Shankar, T.G. McGee, B.L. Kemp, Analysis of spinning spacecraft with wire booms part 3: spin-plane dynamics, maneuvers, and deployment, in: AIAA Guidance, Navigation, and Control Conference, Chicago, IL, 2009.

[18] P.-A. Lindqvist, G. Olsson, R.B. Torbert, B. King, M. Granoff, D. Rau, G. Needell, S. Turco, I. Dors, P. Beckman, J. Macri, C. Frost, J. Salwen, A. Eriksson, L. Åhlén, Y.V. Khotyaintsev, J. Porter, K. Lappalainen, R.E. Ergun, W. Wermeer, S. Tucker, The spin-plane double probe electric field instrument for mms, Space Sci. Rev. 199 (1) (2016) 137–165, https://doi.org/10.1007/s11214-014-0116-9.

[19] J. Fulton, H. Schaub, Dynamics and control of the flexible electrostatic sail deployment, in: 26th AAS/AIAA Space Flight Mechanics Meeting, 2016.

[20] P. Janhunen, A. Quarta, G. Mengali, Electric solar wind sail mass budget model, Geoscientific Instrumentation, Method. Data Syst. 2 (2013) 85–95.

[21] H. Schaub, J.L. Junkins, Analytical Mechanics of Space Systems, third ed., American Institute of Aeronautics and Astronautics, Inc., 1801 Alexander Bell Drive, Reston, Virginia, 2014, pp. 20191–24344.